FUNDAMENTAL AND APPLIED TOXICOLOGY 28, 41–50 (1995)

A Multiple-Path Model of Particle Deposition in the Rat Lung

SATISH ANJILVEL*,[1] AND BAHMAN ASGHARIAN†

*Department of Medicine, Pulmonary Division, Box 3210, Duke University Medical Center, Durham, North Carolina 27710; and
†Chemical Industry Institute of Toxicology, P.O. Box 12137, Research Triangle Park, North Carolina 27709

Received March 25, 1994; accepted April 20, 1995

A Multiple-Path Model of Particle Deposition in the Rat Lung. ANJILVEL, S., AND ASGHARIAN, B. (1995). *Fundam. Appl. Toxicol.* 28, 41–50.

A multiple-path model of particle deposition in the entire rat lower respiratory tract was developed. Deposition in every branch of an asymmetric lung model was calculated using published analytic formulas for efficiencies of deposition by sedimentation, diffusion, and impaction. The conducting airway tree of the model included the entire set of airway measurements for the Long–Evans rat collected by Raabe *et al.* (1976). A model acinus defined by Yeh *et al.* (1979) was attached to each terminal bronchiole. Deposition was calculated for each acinus. Substantial variations in acinar deposition were predicted. These depended on inhaled particle size and tidal volume. The standard deviation in acinar dose was on the order of 0.2 times the average dose. Dose to some pulmonary acini was nearly twice the average acinar dose, suggesting that the geometry of the conducting airway tree of the rat lung may cause a fraction of pulmonary sites to sustain damage from inhaled particles at levels of exposure which cause no effect in the majority of the lung. The results represent a first step toward a complete model of inhaled particle deposition which assesses the effect of heterogeneity of lung structure on deposition at the level of individual airways.

Inhaled particles depositing in the lung can cause pulmonary injury and disease with effects which are often most severe at sites of maximum deposition. Thus, in order to assess the risk from exposure to a given pollutant, one must estimate the distribution of dose throughout the lung. A number of published studies have examined deposition of particles in each generation of simple lung models for humans (Landahl, 1950; Beekmans, 1965; Taulbee and Yu, 1975; Yeh and Schum, 1980; Yu and Diu, 1982) and rats (Schum and Yeh, 1980; Yu and Xu, 1986). These models used a single "typical" path to represent the entire lung or a lobe of the lung. The deposition models for humans typically were based on symmetric structures such as the Weibel model of the lung (Weibel, 1963). The models for the rat used the lung model of Yeh *et al.* (1979).

The advantages of the single-path model are its simplicity and its applicability to an average path without requiring detailed knowledge of the branching structure of the lung. In its usual implementation, deposition in each airway of the typical path is calculated using the deposition efficiency, which is defined as the fraction of particles entering the airway which deposit. Deposition efficiency for fully developed air flow in an airway is approximated by an analytic function of particle diameter, airway geometry, and flow rate. The total deposition in a generation is given by the deposition in that generation of the single path multiplied by the number of airways in that generation for the entire lung. For a symmetric, dichotomous branching tree such as the Weibel model, the latter number is always a power of two. In the model of the rat lung developed by Yeh *et al.* (1979), the number of airways per generation was estimated from anatomical data.

A considerable body of data on lung structure was collected by Raabe *et al.* (1976). These data were the basis of the single-path anatomic models of the whole lung and individual lobes developed by Yeh *et al.* (1979). These anatomical models were the basis of the particle deposition model of Schum and Yeh (1980), who evaluated total and lobar deposition. Significant variation in lobar deposition was predicted, with maximum deposition relative to tissue volume occurring in the right apical lobe.

The inhomogeneity of the branching pattern of the actual lung implies that deposition of particles will not be the same for every airway of a given generation. Moreover, deposition will not be the same in functionally or morphologically similar airways. For example, each terminal bronchiole of the rat lung will receive a dose that depends on both the path from the trachea to the terminal bronchiole and the size of the acinus that the terminal bronchiole ventilates. Because a threshold for noncarcinogenic effects is likely for most pollutants, quantifying variations in dose to sensitive regions of the lung is important: the average dose to the entire alveolar region may be below the threshold for damage, but a significant number of pulmonary acini may receive a dose greater than the threshold value. A single-path deposition model is by its nature unable to predict such variability.

[1] To whom correspondence should be addressed.

0272-0590/95 $12.00

In this paper, we extend the single-path model of Schum and Yeh by defining a multiple-path model of the rat lung which is closely based on actual anatomic data. Deposition is calculated for every airway of our model, thereby allowing the assessment of variation in dose to different sites in the lung, such as the pulmonary acini. This approach is more realistic than the use of a single-path model for two reasons, both of which relate to the distinctly monopodial nature of the rat lung. First, the branching pattern is highly asymmetric, a feature which significantly affects the deposition distribution and is captured only by a multiple-path model. Second, the multiple-path model uses actual airway measurements rather than average values. In the rat lung, the two daughter airways of a given airway can have very different branching angles, diameters, and flow rates. These differences, which can affect deposition significantly, are incorporated in the multiple-path model.

DESCRIPTION OF THE MODEL

Lung Structure

The structural model we used includes the entire set of airways measured by Raabe *et al.* (1976) at the Lovelace Foundation for Medical Education and Research. These data were the basis for the single-path models of Yeh *et al.* (1979). The airway measurements (commonly referred to as the Lovelace database) were taken from lung casts and consist of geometric data for a large collection of the conducting airways of four species, including the Long–Evans rat. The database comprises the branching structure of the tracheobronchial tree and the length, diameter, gravity angle, and branching angle of each airway. For the rat, 4807 airways were measured, including 2404 final airways which had no daughters. The data have been placed in the public domain to facilitate the theoretical modeling of particle deposition and other anatomic studies.

To complete the lung model, pulmonary acini must be attached to the conducting airways. We assumed that all acini have the same structure. Each final airway in the Lovelace airway tree was replaced with a symmetric subtree which represented a pulmonary acinus. The subtree had the terminal airway as its root and eight distal generations of alveolar ducts attached to the root. This acinar structure is similar to the last eight generations of the lung model of Yeh *et al.* (1979), which assumes that there are 2487 terminal bronchioles. We assumed that the lengths and diameters of the alveolar ducts in our model were the same as in the Yeh model. The alveolar volume was chosen so that the total alveolar volumes of the two models were the same. Thus, each pulmonary acinus in our model had 2487/2404 times the alveolar volume of that of the Yeh model. Alveolar volume was assumed to be equally distributed among all alveolar ducts.

The addition of these pulmonary acini implicitly assumes that each of the 2404 final airways are actually terminal bronchioles. In fact, only half of the final airways in the Lovelace dataset were positively identified as terminal bronchioles, while the remainder may have been bronchioles which broke off during trimming or measuring. Nevertheless, this simple method of completing the structure is reasonable because it gives a correct total volume of the rat lung. In addition, our model predictions may be fairly compared with deposition calculations made for the single-path model of Schum and Yeh (1980).

In the report of Raabe *et al.* (1976), the tracheobronchial airway dimensions were assumed to approximate values at end inspiration. On the other hand, the published paper of Yeh *et al.* (1979) assumes that the dimensions correspond to total lung capacity (TLC), which therefore implies a smaller lung geometry at functional reserve capacity (FRC). We ran our simulations with both interpretations of the Lovelace data in order to determine which leads to more accurate predictions of deposition and how sensitive particle deposition is to airway geometry. The alveolar model of Yeh *et al.* (1979) provided dimensions and volumes for a lung inflated to total lung capacity. We first isotropically scaled the airway lengths and diameters of both sets of data to give values corresponding to a lung at FRC. Klingele and Staub (1971) and Hughes *et al.* (1972) showed that lengths and diameters of airways of excised lungs vary roughly in proportion to the one-third power of lung volume. Hahn *et al.* (1976) showed that airway diameters in normal, anesthetized dogs also vary in the same way. Thus, our use of isotropic scaling is a reasonable approximation to dimensional changes that actually occur in the lung. Next, we computed the average of the airway dimensions at FRC and those at end inspiration. These average dimensions, which depend on tidal volume, were used in the model calculations.

The airway tree was stored within a computer in a data structure of connected nodes known as a binary tree. Each node of the binary tree contained data which referred to an airway, including pointers to the nodes for the parent and daughter airways. For many quantities of interest which are defined for each airway, the computation of these quantities must be executed airway by airway in a certain order. A procedure for carrying this out is known as a tree traversal. In some cases, such as the calculation of flow partitioning, the calculation at one node cannot proceed until the calculation at the node's parent has been completed. A traversal satisfying this condition is known as a traversal *down* the tree. In other cases, such as the calculation of distal volume, computation at a node requires completion of the computations at the daughter nodes. A traversal satisfying this condition is known as traversal *up* the tree. We used standard tree traversal algorithms for all airway computations (Knuth, 1973). The same algorithms may be used to traverse any subtree of the airway tree, e.g., a lobe of the lung or a single pulmonary acinus.

Air Flow

For each airway, we first determined the volume distal to it by traversing up the tree (so the trachea was visited last). The distal volume of an airway is defined as the lung volume distal to the proximal end of the airway. Next, we computed the volumetric flow rate in each airway. Since the flow in an airway is determined by the flow in its parent, this computation proceeded by traversing down the tree. We assumed that each region of the lung expands at the same rate, which is equivalent to assuming that flow partitioning is proportional to distal volume. Specifically, given a parent airway p with proximal flow rate $F^{p,0}$ and a daughter airway d, we computed the distal parent flow rate $F^{p,1}$ and the proximal daughter flow rate $F^{d,0}$ using the formulas

$$F^{p,1} = \frac{\mathrm{DV}^p - V^p}{\mathrm{DV}^p} F^{p,0}$$

$$F^{d,0} = \frac{\mathrm{DV}^d}{\mathrm{DV}^p - V^p} F^{p,1}, \tag{1}$$

where V^p denotes the volume of airway p and DV^d and DV^p denote the distal volumes for the daughter and parent airways (see Fig. 1). Note that $F^{p,1} < F^{p,0}$, i.e., flow within an airway is not perfectly conserved. This inequality arises from the change in volume of the airway. The net influx of air into an airway is used to increase the volume of that airway. In practice, the change in flow between the ends of any conducting airway was insignificant because these airways have a large distal volume. However, for the last generations of alveolar ducts, Eq. (1) forces the flow to drop rapidly, as one would expect. The calculation of the position of the front of fresh

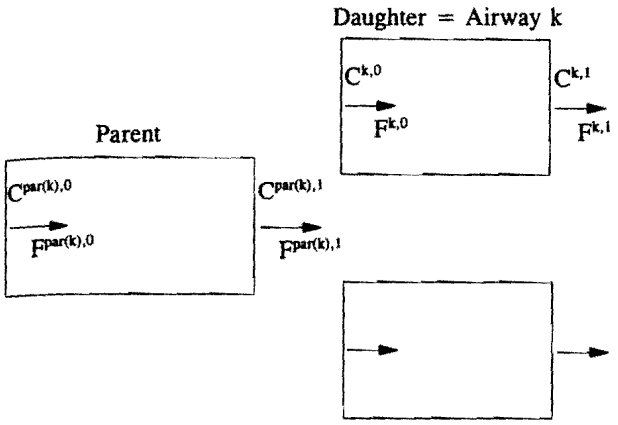

FIG. 1. Flow and concentration quantities defined in the model. In general, $F^{k,0}$ and $F^{k,1}$ are unequal because of airway expansion, and $C^{par(k),1}$ and $C^{k,0}$ are unequal because of deposition by impaction.

inspired air without Eq. (1) can lead to the absurd result that the front moves through the distal wall of alveolar sacs.

We calculated the bulk velocity of air at each end of each airway by dividing the flow at that end by the cross-sectional area of the airway. For an arbitrary airway k, let v_0 and v_1 denote the proximal and distal velocities. Using these velocities, we determined the time when the inspiratory front of fresh air crosses the distal end of the airway, which we denote by t^k_{inh} and refer to as the crossing time for airway k. These times were obtained by traversing down the tree, since the time of crossing for an airway k depends on the time of crossing for its parent par(k). The crossing time t^k_{inh} was calculated by adding to $t^{par(k)}_{inh}$ the time it would take the front to move from the proximal end of the airway to the distal end assuming that the velocity within the airway is a linear function of position along the airway axis. Specifically, the position $x(t)$ of the front while the front is in airway k satisfies the differential equation

$$\frac{dx}{dt} = v_0 + (v_1 - v_0)\frac{x}{L^k}, \tag{2}$$

where L^k is the length of the airway. Solving this equation gives

$$t^k_{inh} = t^{par(k)}_{inh} + \frac{L^k}{v_1 - v_0}\ln\left(1 + \frac{v_1 - v_0}{v_0}\right). \tag{3}$$

If the left-hand side of Eq. (3) is greater than the inspiratory period T_{inh}, then the inspiratory front is within airway k at end inspiration. For this special case, the position of the front within the airway at end inspiration was stored and denoted by x^k_{inh}. Like t^k_{inh}, it is obtained by solving Eq. (2) and is given by

$$x^k_{inh} = L^k\frac{v_1 - v_0}{v_0}\left(\exp\left(\frac{v_1 - v_0}{L^k}T_{inh}\right) - 1\right). \tag{4}$$

Other Parameters

Published experimental measurements of the tidal volume and breathing frequency of rats exhibit great variability (Costa and Tepper, 1988). Two measurements for the Long–Evans rat, by Mauderly *et al.* (1979) and Wiester *et al.* (1988), are at the low and high extremes of published data on minute ventilation per unit body weight for several strains of rat. We used the first study to obtain parameters for quiet breathing: tidal volume = 2.1 ml and breathing frequency = 102 bpm. The second study provided parameter values for rapid breathing: tidal volume = 2.7 ml and breathing frequency = 131 bpm.

The upper respiratory tract affects deposition in the lung by its removal of particles and by its contribution to the anatomical dead space. Upper respiratory tract dead space was computed using published data on area of cross-sections of the nasal cavity of the rat. Numerical integration (using the trapezoidal rule) of the data of Schreider and Raabe (1981) gave a value of 0.35 ml for the upper respiratory tract of a 250-g Sprague–Dawley rat and 0.31 ml excluding nasal pockets. A partial integration of the same data up to the nasopharynx gives excellent agreement with an integration of the data of Gross *et al.* (1982) which was obtained from a 288-g Fischer-344 rat, suggesting that nasal volumes are similar across rat strains. The data of Patra *et al.* (1987), when integrated, give a volume of 0.52 ml for the entire nasal-pharyngeal airway of a 366-g Fischer-344 rat. Interpolating between these values gives a volume of 0.47 ml for a 330-g rat. Assuming that the volume without pockets has the same proportion as that of the Schreider and Raabe rat, we obtain a value of 0.42 ml. In all of our deposition model calculations, the volume of air entering the trachea was assumed to be given by the tidal volume reduced by 0.42 ml.

Deposition Calculations

The calculation of distal volume, flow rates, velocities, and crossing times of the inspiratory front were all preliminary to the calculation of particle deposition. Deposition was calculated during inspiration and expiration for each conducting airway and for every generation of each of the 2404 acini. We first describe the calculation for inspiration, which is somewhat different from that for exhalation.

Inhalation. Inspiratory flow was assumed to be constant. Nasal deposition was estimated using the quasi-empirical formula of Zhang and Yu (1993) which is given in the Appendix. For each airway of the lung, particle concentration, as a function of time, was found at the proximal and distal ends. Let these concentration functions for airway k be denoted by $C^{k,0}_{inh}(t)$ and $C^{k,1}_{inh}(t)$ (see Fig. 1). Since the initial concentration of particles in the airways is assumed to be zero, the concentration at any position is zero before the time that the front of inspired particle-laden air crosses that position. The assumption of steady inspiratory flow and an initial concentration distribution of zero implies that the particle concentration at any position is constant between the time when the front crosses that position and the end of inspiration. Thus, concentration as a function of time during inhalation at an end of an airway is a simple step function taking on two values, one of which is zero. It is completely determined by the time when the front crosses the end of the airway and the value of the concentration after this time and may be written as

$$C^{k,0}_{inh}(t) = \begin{cases} 0 & t < t^{par(k)}_{inh} \\ c^{k,0}_{inh} & t \geq t^{par(k)}_{inh} \end{cases}$$

$$C^{k,1}_{inh}(t) = \begin{cases} 0 & t < t^{k}_{inh} \\ c^{k,1}_{inh} & t \geq t^{k}_{inh} \end{cases} \tag{5}$$

for some constants $c^{k,0}_{inh}$ and $c^{k,1}_{inh}$.

Since the crossing times were already calculated, only determination of these constants remained. This was done by traversing down the airway tree and using the deposition efficiency for each airway. The efficiencies of deposition by sedimentation, impaction, and diffusion were calculated

individually using published analytic formulas. We assumed that these mechanisms act independently. The individual deposition efficiencies are complicated functions of their arguments for which analytic approximations exist in the literature. We used the analytic formulas of Cai and Yu (1988) for impaction, Ingham (1975) for diffusion, and Wang (1975) for sedimentation. These are given in the Appendix.

Each concentration value was calculated after the immediately proximal concentration had been obtained. Assuming that concentration at the distal end of a parent airway was known, the concentration at the proximal end of a daughter was found using the efficiency of impaction. Using the concentration at the proximal end of an airway, the concentration at the distal end was calculated using the efficiencies of sedimentation and diffusion:

$$c_{\text{inh}}^{k,0} = c_{\text{inh}}^{\text{par}(k),1}(1 - \epsilon_i)$$
$$c_{\text{inh}}^{k,1} = c_{\text{inh}}^{k,0}(1 - \epsilon_{\text{sd}}). \tag{6}$$

Here ϵ_i is the deposition efficiency of impaction and depends on the airway dimensions, flow, and particle characteristics. The efficiency ϵ_{sd} is the combined efficiency of sedimentation and diffusion and is defined by $\epsilon_{\text{sd}} = 1 - (1 - \epsilon_s)(1 - \epsilon_d)$, where ϵ_d and ϵ_s are the deposition efficiencies of diffusion and sedimentation, respectively. In the Appendix, ϵ_{sd} is given as a function of dimensionless quantities, but it may also be written in the form $\epsilon_{\text{sd}}(L^k, d^k, f^k, \alpha^k)$, where L^k, d^k, f^k, and α^k are the length, diameter, flow rate, and gravitational angle of airway k. For airways in which the front stops at the end of inspiration, this formula must be modified to account for the effectively shorter airway. Accordingly, we used $\epsilon_{\text{sd}} = \epsilon_{\text{sd}}(x^k, d^k, f^k, \alpha^k)$, where x_k is the stopping position of the front.

The concentration at end inspiration, as a function of the position x along airway k, will be denoted by $C_{\text{inh}}^k(x)$. Since sedimentation and diffusion efficiencies are approximated as linear functions of airway length, this function is best described by an exponential function. However, since the efficiencies are quite small, $C_{\text{inh}}^k(x)$ is reasonably approximated by a linear function. We used the linear function determined by the concentration values at the proximal and distal ends of the airway at end inspiration, $C_{\text{inh}}^{k,0}(T_{\text{inh}})$ and $C_{\text{inh}}^{k,1}(T_{\text{inh}})$. This function must be modified for the case of an airway in which the front stops at the end of inspiration. In this case, the concentration function is assumed to be linear from the proximal end of the airway to the point x_{inh}^k where the front stops.

Once the concentration was obtained as a function of time, we calculated the inspiratory deposition fraction for each airway. The deposition fraction is the ratio of deposited mass to total mass inhaled. The latter quantity is just the product of the ambient concentration and the tidal volume. Deposited mass was computed using the principle of mass balance:

$$m_{\text{dep}}^k = m_{\text{init}}^k + m_{\text{in}}^k - m_{\text{out}}^k - m_{\text{rem}}^k, \tag{7}$$

where (omitting the superscript k), m_{dep} is the deposited mass, m_{init} is the mass initially in the airway, m_{in} and m_{out} are the masses entering and leaving the airway during inspiration, and m_{rem} is the undeposited mass in the airway at the end of inspiration. The deposited mass must be obtained indirectly using Eq. (7) rather than directly using deposition efficiencies because the efficiency formulas assume that every particle either deposits or exits. In our case, some particles enter airway k but do not have the opportunity to exit before the inspiratory period ends. The fraction of these particles that do not deposit is m_{rem}. The sum of m_{rem} over all airways gives the total suspended mass at end inspiration. These particles subsequently are exhaled or deposited during exhalation. Each of the terms on the right-hand side of Eq. (7) can be evaluated if the concentration functions in Eq. (5) are known. For inspiration, the initial mass is zero. The mass entering is given by

$$m_{\text{in}}^k = \int_0^{T_{\text{inh}}} F^{k,0} C_{\text{inh}}^{\text{par}(k),1}(t)dt = c_{\text{inh}}^{\text{par}(k),1}(T_{\text{inh}} - t_{\text{inh}}^{\text{par}(k)})F^{k,0}, \tag{8}$$

where $F^{k,0}$ is the air flow entering airway k, and the last equality follows from Eq. (5). Similarly, the mass which leaves is given by

$$m_{\text{out}}^k = \int_0^{T_{\text{inh}}} F^{k,1} C_{\text{inh}}^{k,1}(t)dt = c_{\text{inh}}^{k,1}(T_{\text{inh}} - t_{\text{inh}}^k)F^{k,1}. \tag{9}$$

The mass remaining at end inspiration is determined by integrating the concentration distribution and is approximated by

$$m_{\text{rem}} = A^k \int_0^{L^k} c_{\text{inh}}^{k,1}(x)dx \approx \frac{c_{\text{inh}}^{k,0} + c_{\text{inh}}^{k,1}}{2} L^k A^k, \tag{10}$$

where A^k is the cross-sectional area of airway k. These formulas are also valid when the airway is one where the front stops, except that L^k must be replaced by x_{inh}^k, the distance from the proximal end to the point where the front stops. Note that in using Eqs. (8) and (9), particles that deposit at the bifurcation of an airway are considered to contribute to the deposition fraction for one of the daughter airways.

Exhalation. In principle, the deposition fractions for exhalation may be calculated in a manner similar to that for inhalation. The principal difference is that there is a nonzero initial distribution of particles in the airways. If the particle concentration is known as a function of time at both ends of airway k, one may calculate m_{in} and m_{out} using analogues of the first equalities in Eqs. (8) and (9). However, because the concentration distribution is nonzero at the start of exhalation, the concentration functions which are the expiratory analogues of $C_{\text{inh}}^{k,0}$ and $C_{\text{inh}}^{k,1}$ are not step functions of the form given in Eq. (5), but are more general functions of time. These functions must be approximated numerically with considerable accuracy, since otherwise the error from numerical computation of the integrals in Eqs. (8) and (9) will overwhelm the calculation of m_{dep} in Eq. (7).

We chose not to use the above method of calculation; instead, we calculated the masses directly using a simpler method in which deposition fractions are calculated directly from Eq. (7). The air flow and crossing time for each airway were first computed, as in the case of inhalation. Since no pause between inhalation and exhalation was modeled, we defined the initial mass m_{init} for exhalation to equal the remaining mass m_{rem} calculated for inhalation. Also, we made the simplifying assumption that m_{rem} for exhalation is zero. This is equivalent to assuming that every inhaled particle either is exhaled or deposits by the end of exhalation and follows because longitudinal dispersion is not incorporated in the model. Deposition by impaction was not modeled. Thus, of the mass m_{in} entering airway k, the fraction which exits is $(1 - \epsilon_{\text{sd}})m_{\text{in}}$. Of the mass initially in the airway, the fraction which exits is approximately $(1 - \epsilon_{\text{sd}}/2)m_{\text{rem}}$. The efficiency $\epsilon_{\text{sd}}/2$ is the average of the efficiency at the proximal end (i.e., 0) and the efficiency at the distal end (i.e., ϵ_{sd}). Thus,

$$m_{\text{in}}^k = m_{\text{out}}^{d_1} + m_{\text{out}}^{d_2}$$
$$m_{\text{out}}^k = (1 - \epsilon_{\text{sd}})m_{\text{in}}^k + \left(1 - \frac{\epsilon_{\text{sd}}}{2}\right)m_{\text{rem}}^k, \tag{11}$$

where d_1 and d_2 are the daughters of airway k. The first equation holds because impaction is neglected. Equation (11) expresses the masses entering and leaving the airway in terms of the initial data and the corresponding masses for the daughter airways. For those airways where the front stops, and for all airways distal to them, m_{in} is zero. Thus, m_{in} and m_{out} can be found by traversing up the airway tree and using Eq. (11). After computing these masses, m_{dep} was obtained for each airway using Eq. (7). For airways in which the inspiratory front stops, the efficiency must be corrected in the same way as in the calculation of inspiratory deposition.

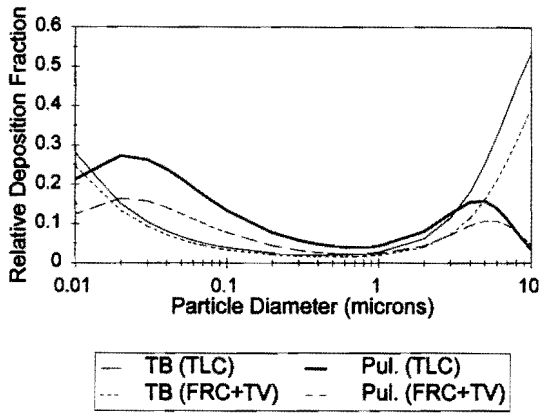

FIG. 2. Fraction of particles entering the trachea that deposit in the tracheobronchial (TB) and pulmonary (Pul) regions during quiet breathing as a function of particle diameter. Deposition was computed assuming the Lovelace data represent total lung capacity (TLC) and assuming they represent end inspiration (FRC + TV). Tidal volume = 2.1 ml; breathing frequency = 102 bpm; particle density = 1.0 g/cm^3.

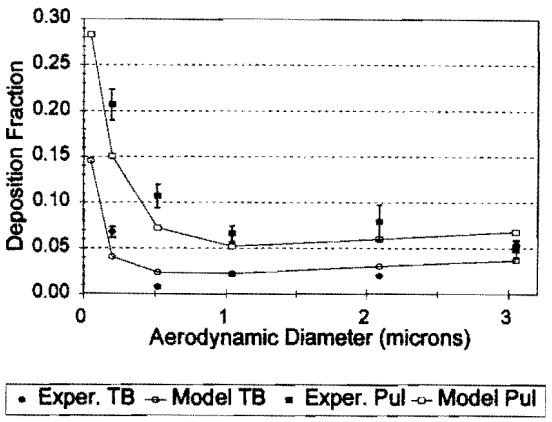

FIG. 3. Comparison of model predictions with experimental data. Experimental data and breathing parameters are from Raabe *et al.* (1975). Tidal volume = 2.3 ml; breathing frequency = 68 bpm; particle density = 2.2 g/ml.

RESULTS

We first evaluated tracheobronchial and pulmonary deposition fractions for the entire lung relative to the mass entering the trachea. These are shown as a function of particle diameter for quiet breathing in Fig. 2. Tracheobronchial and pulmonary deposition were computed for the small airway model in which the Lovelace data represent dimensions at TLC and for the large airway model in which the Lovelace data represent dimensions at FRC + TV, where TV is tidal volume. Note that there is substantially greater pulmonary deposition with the smaller airway model.

The smaller model, which uses airway dimensions similar to those of the single-path model of Schum and Yeh (1980), agreed well with the predictions of this model. In particular, both models predicted minimum values of total and pulmonary deposition for particles with diameters between 0.5 and 1.0 μm, a fact confirmed by Raabe *et al.* (1975). Both also predict pulmonary deposition of large particles, relative to mass entering the trachea, to be maximized for particle diameters between 4 and 5 μm. (Fig. 1 of the Schum and Yeh paper shows the peak occurring for smaller particles, but their graph includes removal by nasal deposition.)

We compared the model's predictions with the experimental data of Raabe *et al.* (1975) which also used the Long–Evans rat. In this case, nasal deposition was estimated using data from the same study. We computed the predicted deposition fraction using the same breathing parameters and particle characteristics as in the experimental study. Both the large and small airway models were used. We found much better agreement with experimental data when we used the small model. For this reason, all other model calculations were performed using the small model which uses the Lovelace data as measurements at TLC. This is the only instance in which the value of a model parameter was chosen to improve agreement of the model's predictions with experimental data. The results are shown in Fig. 3. There is good general agreement between predicted and experimental deposition in the tracheobronchial and pulmonary regions. The agreement for total deposition is remarkable considering the variability in the experimental data and the simplifying assumptions of the model. Note that the Raabe measurements for the smallest particle size are plotted for 0.2 μm. In fact, the sample of the smallest particles was a mixture of particles of aerodynamic diameter 0.2 and 0.05 μm in unknown proportions. We have plotted the predicted deposition for both of these sizes; the actual experimental deposition should be and is between these values.

We next investigated regional variations in deposition at the lobar level. The average acinar deposition fraction for each lobe was computed by dividing the lobar deposition fraction by the number of acini per lobe. The results are shown for quiet and rapid breathing in Fig. 4. Figure 4 refers to a 1-μm particle, but the relative deposition numbers were virtually identical for all particle sizes. Substantially higher relative deposition occurred in the right apical lobe. Both the insensitivity of relative lobar deposition to particle size and the enhanced deposition in the right apical lobe were also predicted by Schum and Yeh (1980) and measured by Raabe *et al.* (1975). Our model predicted greater deposition in the right cardiac lobe, while substantially lower deposition was predicted for the left apical lobe. Raabe *et al.* (1975) did not observe increased deposition in the right cardiac lobe, and deposition was not measured in the left apical lobe alone. In addition,

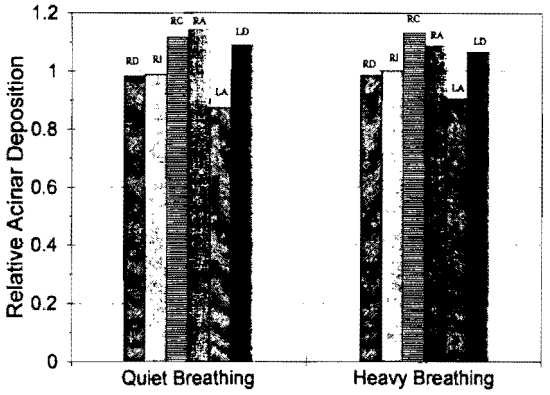

FIG. 4. Average acinar deposition for each lung lobe divided by the average acinar deposition for the whole lung. Particle diameter = 1 μm; density = 1.0 g/cm^3. For heavy breathing, tidal volume = 2.7 ml; breathing frequency = 131 bpm. RD, right diaphragmatic; RI, right intercostal; RA, right apical; RC, right cardiac; LD, left diaphragmatic; LA, left apical.

we found that the variation in relative lobar deposition was almost independent of breathing frequency and fairly insensitive to tidal volume, as seen in Fig. 4.

To examine regional variations in deposition in more detail, we computed the deposition to each individual acinus. This resulted in 2404 deposition fractions which together form the acinar deposition distribution. The simplest measure of variation in a distribution is the standard deviation. The standard deviation of acinar deposition normalized by mean acinar deposition (coefficient of variation) as a function of particle diameter is presented in Fig. 5 for quiet and heavy breathing. The coefficient of variation of acinar deposition is smallest for particles between 0.03 and 0.8 μm in diameter. For these particles, the coefficient of variation

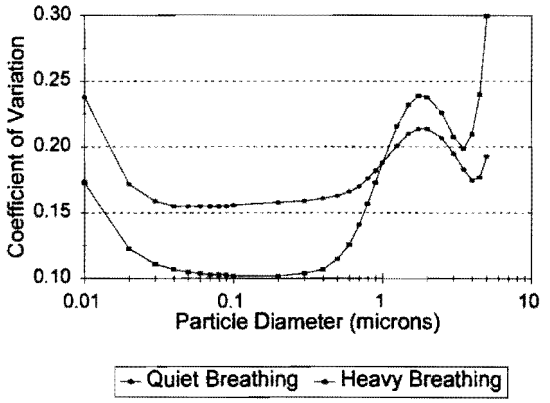

FIG. 5. Standard deviation of the acinar dose distribution divided by the mean of the acinar dose distribution as a function of particle size for quiet breathing. Tidal volume = 2.1 ml; breathing frequency = 102 bpm; particle density = 1.0 g/cm^3.

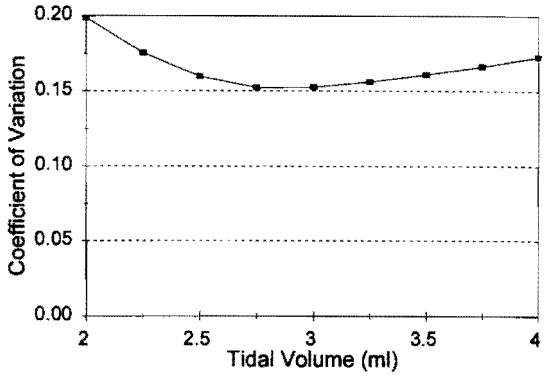

FIG. 6. Standard deviation of the acinar dose distribution divided by the mean of the distribution as a function of tidal volume. Particle diameter = 1 μm; density = 1.0 g/cm^3; breathing frequency = 102 bpm.

is significantly larger for quiet breathing, while for larger particles it is larger for heavy breathing. An important fact that is not indicated by the figure is that although the *relative* pulmonary variation increases with tidal volume for small particles, the *absolute* variation in deposited mass increases with heavy breathing for all particle sizes because the total deposited mass increases substantially.

As with variations in lobar deposition, the standard deviation of the acinar deposition distribution was essentially independent of breathing frequency. Its dependence on tidal volume is shown in Fig. 6 for a 1-μm particle. The corresponding curves for other particle sizes are all very similar to the curve in Fig. 6.

Figure 7 shows the actual deposition distribution for each

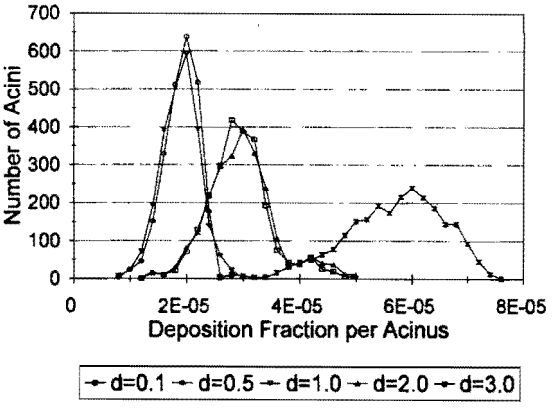

FIG. 7. Acinar dose distribution for five different particles inhaled during quiet breathing. For each particle size, the markers have a horizontal spacing of 2.0×10^{-6}. The ordinate of a marker with abscissa x gives the number of acini whose deposition fraction is greater than $x - 2.0 \times 10^{-6}$ and less than or equal to x. Such distributions are traditionally represented by a histogram with a bar corresponding to each marker, but markers and lines are used for better discernment. Particle density = 1.0 g/cm^3.

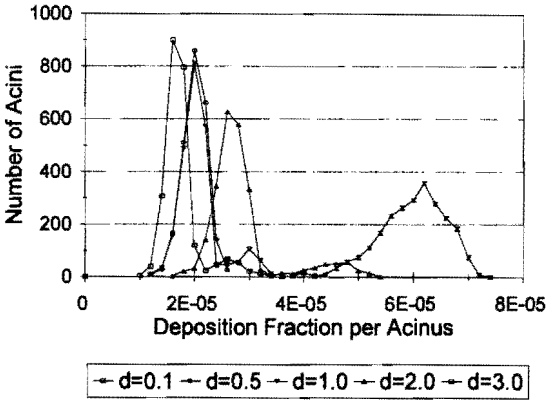

FIG. 8. Acinar dose distribution for five different particles inhaled during heavy breathing.

of five different particle sizes, assuming quiet breathing. Nasal deposition was modeled using the empirical formula of Zhang and Yu (1993). Each curve should be interpreted as a histogram since the number of acini is finite. The means of these distributions, when multiplied by 2404, correspond to points on the pulmonary deposition curve in Fig. 2. The variances of the distributions increase as the mean increases, as predicted by the graph in Fig. 5. The right-hand tail of the distribution of a 3.0-μm particle is much more pronounced than that of a 0.1-μm particle. This is also true of the 2.0-μm particle, while the smaller particles have more compact deposition histograms. Pulmonary acini that make up the tail of these distributions receive much higher deposition than the average for all acini.

The presence of a large right-hand tail in the acinar deposition distribution for larger particles is even more apparent for deeper breathing. This is seen in Fig. 8, which presents the deposition distributions of Fig. 7 but with the tidal volume increased by 50% to 3.2 ml. The tails of the distributions of the 2.0-μm and 3.0-μm particles are much greater than in Fig. 7 and now have a small peak, making the distributions slightly bimodal. The center of each distribution is now more sharply peaked, which explains why the larger tails do not increase the normalized standard deviation. Acini at the extreme tail of the distribution for larger particles receive approximately 1.8 times the average acinar deposition.

DISCUSSION AND CONCLUSIONS

This study is a first step toward a theoretical model of inhaled particle deposition which models heterogeneity of lung structure and its effect on deposition. The principal conclusions of this study are summarized below.

1. Theoretical predictions of particle deposition using the Lovelace dataset agree best with experimental data when the data are assumed to represent the lung at TLC, not at end inspiration. Pulmonary deposition was quite sensitive to the dimensions of the conducting airway tree.

2. Substantial variations in relative lobar and acinar deposition occur in the monopodial conducting airway tree of the Long–Evans rat based on the Lovelace data. These variations occur even though the model assumes that all pulmonary acini have the same structure.

3. The coefficient of variation of the acinar deposition distribution ranges from 0.10 to 0.25 for respirable particles with the largest values occurring for very large and very small particle sizes. It is independent of breathing frequency and, for submicron particles, decreases with increasing tidal volume.

4. The acinar deposition distributions for larger particles have significant tails, especially for larger tidal volumes. Acini which belong to the tail of the distribution can receive deposition almost twice as great as the average acinar deposition.

5. The development of site-specific models of particle deposition requires more data on the anatomy of the upper and lower respiratory tracts and more accurate measurements of tidal volume. The validation of such models requires data from experiments designed to measure regional deposition data.

The most significant prediction of this model is that a small fraction of pulmonary acini can receive nearly twice the average acinar deposition because of the asymmetry of the conducting airway tree. Such acini may be particularly susceptible to toxic injury from inhaled particles because they receive increased deposition and also because the greater deposition may locally overload alveolar clearance mechanisms. As a result, deposited particles at these acini may reside much longer than at acini receiving average deposition, thereby making the difference in tissue dose even greater. The susceptibility of such sites in humans may be less pronounced because of the more symmetric branching pattern in the human lung. Another interesting prediction of this model is that deposition should be significantly higher in the left apical lobe. Experimental verification of this prediction would provide additional corroboration of the validity of this model.

The sensitivity of deposition variation to tidal volume and, by implication, to anatomical dead space has important implications for particle dosimetry experiments in which dose–response relationships are sought. Because of the great individual variability in these parameters, accurate measurements of nasal-pharyngeal and tracheobronchial volumes, as well as the tidal volumes when resting and active, ideally should be measured in the animals which are being exposed to test particles. Practical considerations may, of course, make this unfeasible.

The Lovelace database does not provide data on every airway of the rat lung. The use of these data as a complete tracheobronchial tree undoubtedly introduces some error into the model. It is difficult to judge how this error affects the theoretical model's estimate of variation in the deposition distribution, since this depends on precisely how the Lovelace data fail to provide a complete lung structure. For example, if longer paths were much more likely to break during casting than shorter paths, then the Lovelace data would underestimate the variation in airway path length in the lung which, in turn, would lead to an underestimate of the variation in particle deposition. On the other hand, if the probability of breakage had been independent of path length, then use of the Lovelace data would not result in this type of bias.

A more important source of inaccuracy in the theoretical model is the simplifying assumption that all acini are the same size. Reconstructions of rat pulmonary acini by Mercer *et al.* (1990) show that there are large variations in the size and branching structure of acini and that these have a significant effect on reactive gas dosimetry. Including such variation in our model would refine the accuracy of the model predictions. Variations in acinar geometry are expected to increase the predicted variation in regional deposition. This topic will be addressed in a future study.

APPENDIX

Below we present the formulas used to calculate nasal deposition and airway deposition efficiency by the mechanisms of impaction, diffusion, and sedimentation. In each case, the efficiency is expressed as a function of dimensionless quantities.

Nasal Deposition

From Zhang and Yu (1993),

$$\epsilon_{\text{nasal}} = \left[\frac{(d_a^2 Q)^\alpha}{C + (d_a^2 Q)^\alpha}\right]^\beta,$$

where d_a is the aerodynamic diameter, Q is the flow rate, and $\alpha = 2.553$, $\beta = 0.627$, and $C = 10^5$ are empirically obtained constants.

Impaction and Interception

From Cai and Yu (1988), the deposition efficiency for impaction is given by

$$\epsilon_i = \epsilon_i\left(\alpha, \frac{R}{R_0}, \text{St}_0\right) = \frac{8 \sin \alpha f_1\left(\alpha, \frac{R}{R_0}\right)}{\frac{R}{R_0} f_0\left(\alpha, \frac{R}{R_0}\right)} \text{St}_0,$$

where

$$f_0\left(\alpha, \frac{R}{R_0}\right) = \pi - \left(\frac{\pi}{4} + \left(\frac{5}{4}\pi - \frac{8}{3}\right)\cos^2\alpha\right)\left(\frac{R}{R_0}\right)^2$$

$$f_1\left(\alpha, \frac{R}{R_0}\right) = 1 + \left(-\frac{1}{3} + \left(\pi - \frac{11}{3}\right)\cos^2\alpha - \frac{\sin\alpha}{3}\right) \times \left(\frac{R}{R_0}\right)^2 + \left(\left(\frac{2}{3} - \frac{\pi}{8}\right)\cos^2\alpha + \frac{\sin^2\alpha}{5} + \left(6 - \frac{15}{8}\pi\right)\cos^4\alpha + \left(\frac{7}{15} - \frac{\pi}{8}\right)\sin^2\alpha \cos^2\alpha\right)\left(\frac{R}{R_0}\right)^4$$

and α is the bifurcation angle, R is the radius of the daughter, R_0 is the radius of the parent, and St_0 is the particle Stokes number. The latter quantity is given by

$$\text{St}_0 = \frac{\rho C_s d_p^2 u_0}{36 \mu R_0},$$

where ρ is the particle density, C_s is the slip correction factor, d_p is the particle diameter, μ is the air viscosity, and u_0 is the average flow velocity in the parent airway.

Diffusion

From Ingham (1975), the efficiency of diffusion is given by

$$\epsilon_d = \epsilon_d(\Delta) = 1 - 0.819e^{-14.63\Delta} - 0.0976e^{-89.22\Delta} - 0.0325e^{-228\Delta} - 0.0509e^{-125.9\Delta^{2/3}}$$

with

$$\Delta = \frac{DL}{4UR^2},$$

where D is the diffusion coefficient, L is the length of the airway, U is the average air velocity in the airway, and R is the radius of the airway.

Sedimentation

Deposition efficiency by sedimentation is obtained from Wang (1975). If α is the angle of inclination of the airway with respect to the horizontal (so $0 < \alpha < \pi/2$), then the results depend on whether the flow is uphill or downhill.

Flow uphill. There are three cases depending on the value of α.

For

$$0 < \alpha < \frac{\pi}{2} - \frac{2R}{9L}\left(\frac{2v_s}{3u_0}\right)^{1/2},$$

$$\epsilon_s = \epsilon_s(\gamma, \sigma)$$

$$= \frac{1}{\pi}\left(3\sqrt{\sigma(1-\sigma)} + \sin^{-1}\sqrt{1-\sigma} + (1-9\sigma^2)\right.$$

$$\left.\times \sin^{-1}\sqrt{\frac{1-\sigma}{1+3\sigma}}\right) - \frac{2}{\pi}\left(\sqrt{\gamma(1-\gamma)}(1-2\gamma) + \sin^{-1}\right.,$$

where

$$\gamma = \left(\frac{3v_sL}{8u_0R}\cos\alpha\right)^{2/3} \Big/ \left(1 - \frac{v_s}{2u_0}\sin\alpha\right)$$

$$\text{and } \sigma = \frac{v_s}{6u_0}\sin\alpha \Big/ \left(1 - \frac{v_s}{2u_0}\sin\alpha\right)$$

and

$$v_s = \frac{\rho d_p^2 g C_s}{18\mu}$$

is the settling velocity of the particle.

For

$$\frac{\pi}{2} - \frac{2R}{9L}\left(\frac{2v_s}{3u_0}\right)^{1/2} < \alpha < \frac{\pi}{2} - \frac{Rv_s}{8u_0L},$$

$$\epsilon_s = \epsilon_s(\sigma, \zeta_0) = \frac{1+3\sigma}{\pi}\sqrt{1-\zeta_0^2}\left(\zeta_0 + \frac{4\gamma^{3/2}}{\sqrt{1+3\sigma}}\right.$$

$$\left.-\sqrt{\zeta_0^2 - \frac{3\sigma}{1+3\sigma}}\right) + \frac{1-9\sigma^2}{\pi}\sin^{-1}\sqrt{1-\zeta_0^2}$$

$$-\frac{1}{\pi}\sin^{-1}\sqrt{(1+3\sigma)(1-\zeta_0^2)},$$

where

$$\zeta_0 = \frac{Rv_s\sin^2\alpha}{8u_0L\cos\alpha} - \frac{1}{16}\sqrt{\frac{v_s}{6u_0}\sin\alpha} + \frac{7L}{8R}\cot\alpha.$$

For

$$\alpha > \frac{\pi}{2} - \frac{Rv_s}{8u_0L},$$

$$\epsilon_s = 0.$$

Flow downhill.

$$\epsilon_s = \epsilon_s\left(\frac{v_s}{u_0}, \frac{L}{R}, \alpha\right)$$

$$= -\frac{2}{\pi}\sin^{-1}\sqrt{1-\zeta_1^2} - \frac{\sqrt{1-\zeta_1^2}}{\pi(1+(v_s/u_0)\sin\alpha)}$$

$$\times\left(\frac{3v_sL}{2u_0R}\cos\alpha - \left(2 + \frac{v_s}{u_0}\sin\alpha\right)\zeta_1\right),$$

where

$$\zeta_1 = \left(\frac{\frac{3v_sL}{8u_0R}\cos\alpha}{1 + \frac{3v_s}{4u_0}\sin\alpha}\right)^{1/3}.$$

ACKNOWLEDGMENTS

The authors thank Richard C. Graham for providing them with a copy of the Lovelace data and Dr. Fred Miller for helpful advice and suggestions. This work was supported in part by the Chemical Industry Institute of Toxicology and the U.S. Environmental Protection Agency. Although the research described in this article has been funded in part by the EPA under Assistance Agreement CR820450 to Duke University Medical Center, it has not been subjected to the Agency's peer and administrative review and therefore may not necessarily reflect the views of the Agency, and no official endorsement should be inferred.

REFERENCES

Beekmans, J. M. (1965). The deposition of aerosols in the respiratory tract. I. Mathematical analysis and comparison with experimental data. *Can. J. Physiol. Pharmacol.* **43,** 157–172.

Cai, F.-S., and Yu, C. P. (1988). Inertial and interceptional deposition of spherical particles and fibers in bifurcating airways. *J. Aerosol Sci.* **19,** 679–688.

Costa, D. L., and Tepper, J. S. (1988). Approaches to lung function assessment in small mammals. In *Toxicology of the Lung,* pp. 147–173. Raven Press, New York.

Gross, E. A., Swenberg, J. A., Fields, S., and Popp, J. A. (1982). Comparative morphometry of the nasal cavity in rats and mice. *J. Anat.* **135,** 83–88.

Hahn, H. L., Graf, P. D., and Nadel, J. A. (1976). Effect of vagal tone on airway diameters and on lung volume in anesthetized dogs. *J. Appl. Physiol.* **41,** 581–589.

Hughes, J. M. B., Hoppin, F. G., Jr., and Mead, J. (1972). Effect of lung inflation on bronchial length and diameter in excised lungs. *J. Appl. Physiol.* **32,** 25–35.

Ingham, D. B. (1975). Diffusion of aerosols from a stream flowing through a cylindrical tube. *J. Aerosol Sci.* **6,** 125–132, 1975.

Klingele, T. G., and Staub, N. C. (1971). Terminal bronchiole diameter changes with volume in isolated, air-filled lobes of the cat lung. *J. Appl. Physiol.* **30,** 224–227.

Knuth, D. E. (1973). *The Art of Computer Programming,* Vol. I, Addison-Wesley, Reading, MA.

Landahl, H. D. (1950). On the removal of air-borne droplets by the human respiratory tract. I. The lung. *Bull. Math. Biophys.* **12,** 43–56.

Mauderly, J. L., Tesarek, J. E., and Sifford, L. J. (1979). Respiratory measurements of unsedated small laboratory mammals using nonrebreathing valves. *Lab. Anim. Sci.* **29,** 323–329.

Mercer, R. R., Anjilvel, S., Miller, F. J., and Crapo, J. D. (1990). Inhomogeneity of ventilatory unit volume and its effects on reactive gas uptake. *J. Appl. Physiol.* **70,** 2193–2205.

Patra, A. L., Ménache, M. G., Shaka, N. B., and Gooya, A. (1987). A morphometric study of nasal-pharyngeal growth for particle deposition in the rat. *Am. Ind. Hyg. Assoc. J.* **48,** 556–562.

Raabe, O. G., Yeh, H.-C., Newton, G. J., Phalen, R. F., and Velasquez, D. J. (1975). Deposition of inhaled monodisperse aerosols in small rodents. In *Inhaled Particles IV* (W. H. Walton, Ed.), pp. 3–21. Pergamon, Oxford.

Raabe, O. G., Yeh, H.-C., Schum, G. M., and Phalen, R. F. (1976). *Tracheobronchial Geometry: Human, Dog, Rat, Hamster,* LF-53. Lovelace Foundation, Albuquerque, New Mexico.

Schreider, J. P., and Raabe, O. G. (1981). Anatomy of the nasal-pharyngeal airway of experimental animals. *Anat. Rec.* **200,** 195–205.

Schum, M., and Yeh, H.-C. (1980). Theoretical evaluation of aerosol deposition in anatomical models of mammalian lung airways. *Bull. Math. Biol.* **42,** 1–15.

Taulbee, D. B., and Yu, C. P. (1975). A theory of aerosol deposition in the human respiratory tract. *J. Appl. Physiol.* **38,** 77–84.

Wang, C. S. (1975). Gravitational deposition of particles from laminar flows in inclined channels. *J. Aerosol Sci.* **6,** 191–204.

Weibel, E. R. (1963). *Morphometry of the Human Lung,* Springer-Verlag, Berlin.

Wiester, M. J., Tepper, J. S., King, M. E., Ménache, M. G., and Costa, D. L. (1988). Comparative study of ozone (O_3) update in three strains of rat and in the guinea pig. *Toxicol. Appl. Pharmacol.* **96,** 140–146.

Yeh, H.-C., and Schum, G. M. (1980). Models of human lung airways and their application to inhaled particle deposition. *Bull. Math. Biol.* **42,** 461–480.

Yeh, H.-C., Schum, G. M., and Duggan, M. T. (1979). Anatomic models of the traceobronchial and pulmonary regions of the rat. *Anat. Rec.* **195,** 483–492.

Yu, C. P., and Diu, C. K. (1982). A comparative study of aerosol deposition in different lung models. *Am. Ind. Hyg. Assoc. J.* **43,** 54–65.

Yu, C. P., and Xu, G. B. (1986). Predictive models of deposition of diesel exhaust particulates in human and rat lungs. *Aerosol Sci. Technol.* **5,** 337–347.

Zhang, L., and Yu, C. P. (1993). Empirical equations for nasal deposition of inhaled particles in small laboratory animals and humans. *Aerosol Sci. Technol.* **19,** 51–56.